This is a post-peer-review, pre-copyedit version of an article published in Engineering Structures. The final authenticated version is available online at: https://doi.org/10.1016/j.engstruct.2021.112439

Integrated Framework to Structurally Model Unreinforced Masonry Italian Medieval Churches from Photogrammetry to Finite Element Model Analysis through Building Information Modeling

David Pirchio[a]*, Kevin Q. Walsh[a,b], Elizabeth Kerr[a], Ivan Giongo[c], Marta Giaretton[d], Brad D. Weldon[e,b], Luca Ciocci[f], and Luigi Sorrentino[g]

[a]Department of Civil and Environmental Engineering & Earth Sciences, University of Notre Dame, South Bend, Indiana, USA; [b]Frost Engineering & Consulting, Mishawaka, Indiana, USA; [c]Department of Civil, Environmental and Mechanical Engineering, University of Trento, Trento, Italy; [d]Dizhur Consulting, Auckland, New Zealand; [e]Department of Civil Engineering, New Mexico State University, Las Cruces, New Mexico, USA; [f]Office for Cultural Heritage and Religious Buildings of the Diocese of Anagni-Alatri, Italy; [g]Department of Structural and Geotechnical Engineering, Sapienza University of Rome, Roma, Italy.

*e-mail: dpirchio@nd.edu; mail: Department of Civil and Environmental Engineering & Earth Sciences, University of Notre Dame, 156 Fitzpatrick Hall of Engineering, Notre Dame, IN 46556, USA

Abstract

A novel, integrated framework is proposed to assess the vulnerability of a case study unreinforced masonry (URM) Italian church by applying interacting modern tools including unmanned aircraft systems (UAS), “structure from motion” (SfM) photogrammetric survey equipment and software, and finite element method (FEM) analysis software in a complete heritage building information model (HBIM). The FEM model was used to perform both a modal response spectrum analysis and a validation pushover using stiffness adaptation analysis (SAA) to investigate the global behavior of the church and to identify the most critical local mechanisms for collapse potential. Once the most vulnerable components of the church were identified, macro-block analysis was used to estimate the capacity of these collapse mechanisms. Macro-block analysis is well established in the field and was proposed for use as one step in the overall proposed methodology with the aim of providing a holistic methodology that is sophisticated enough to identify the most vulnerable elements of URM churches, but also practical and efficient enough to be applied by practitioners. Traditionally, obtaining the necessary geometric information to correctly conduct the macro-block analysis of such complex buildings requires time-demanding and expensive surveying campaigns. Furthermore, accurately and precisely identifying the local failure mechanisms most influential to macro-block behavior is numerically demanding. The novelty of the current research detailed herein regards a proposed comprehensive seismic vulnerability analysis of historic URM churches with increased efficiency and accuracy of surveying and capacity modeling using modern tools in a fashion approachable by practitioners.

Keywords: URM churches; unmanned aircraft systems; structure from motion; photogrammetry; dense points cloud; HBIM; macro-blocks; FEM; modal response spectrum; macro-block crack lines.

1. Introduction

Unreinforced masonry (URM) churches are a critical component of Italian Heritage due to their inherent historic value, ongoing community usage, and the large quantity and significance of artwork housed therein. According to Cagnana [1], most of the remaining Medieval churches in Italy were constructed using unreinforced masonry (URM) due to the prominence of URM construction techniques during the High and Late Middle Ages, as well as the known durability of URM. Furthermore, URM churches are also present in other countries with regions of high seismicity [2]. URM churches are usually composed of slender vertical elements which are especially vulnerable to damage and collapse under high lateral load demands, and the vulnerability of this construction type was widely observed during past earthquakes such as in Friuli-Venezia Giulia in 1976 [3], in Basilicata and Campania in 1980 [4], in Umbria-Marche in 1997 [5, 6], in L'Aquila in 2009 [7, 8, 9], in Emilia- Romagna in 2012 [10, 11], and in central Italy in 2016 [12, 13].

A holistic risk assessment methodology to guide the decision-making processes of the dioceses for prioritizing detailed assessments and retrofitting interventions was previously proposed [14]. Given the regional scale of this holistic methodology and its rapid application, the holistic methodology relied on simplistic, approximate methods to quantify structural vulnerabilities with the intention that churches with high holistic risk indices would subsequently be prioritized for more detailed vulnerability assessment. The church of *Santa Maria Maggiore* in Alatri (Figure 1) was identified as the church having the highest risk rating, i_R, among the seven churches in the Lazio region considered in the holistic study (Pirchio, et al. 2020a), and was thus identified as the highest priority candidate in the region for the subsequent detailed assessment as described herein. The church is located in the main square of the city, in the diocese of Anagni – Alatri (province of Frosinone). Construction of the church was completed in the 13th century, and it was constructed atop the ruins of a pagan temple dating from the 5th century A.D. The church was constructed with masonry in square-cut stones and lime-based mortar. It has three groin-vaulted naves (a main nave and two lateral aisles), no transept, and a vaulted apse divided from the rest of the church by a triumphal arch. Hemispherical-vaulted chapels were constructed on the south side of the church, while buttresses were placed by the north lateral wall. The main façade has three points of ingress (corresponding to each nave) and a large circular rose-window on top of the main entrance. The bell tower is attached to the body of the church, with two sides atop the façade and the north lateral wall of the main church structure, while the other two sides of the bell tower are supported by independent walls with internal arches. A reinforced concrete bond beam sits atop the exterior walls, supporting timber trusses forming the pitched roof.

Figure 1 - Church of Santa Maria Maggiore, Alatri, Lazio (Italy).

The material mechanical properties (e.g., masonry compressive strength, shear strength, elastic modulus, etc.) often govern the in-plane and dynamic behavior of URM structures [15, 16, 17] and were determined for the case study church using an aggregation of non-destructive test techniques conducted by Pirchio, et al. [18]. The geometric properties of the building components are the governing parameters for the out-of-plane behavior of URM structures [19, 15, 20]. Thus, an adequate understanding of the three-dimensional (3D) configuration of the church is necessary for a proper detailed vulnerability analysis.

The proposed framework addresses the complete modeling procedure of a URM church starting from the acquisition of the geometric configuration to the global structural analysis of the church and finally then the local structural capacity analysis of its components using “macro-blocks.” The framework was developed with the primary aim of being generalizable for similar cases and applicable using software widely employed in engineering practice. Four steps describe the framework generally:

- *Step 1*: Acquisition of the geometry of the church via "structure from motion" (SfM) photogrammetry-based surveys using unmanned aircraft systems (UAS) and the development of a dense point cloud;
- *Step 2*: Development of a solid 3D model comprising geometric information, material properties, and various other risk-related information collected from site investigations [14, 18]. This information is aggregated into a complete heritage building information model (HBIM);
- *Step 3*: Structural analysis of the church to identify the components most likely to experience high demands using finite element method (FEM) analysis software to carry out both a modal response spectrum analysis and a validation pushover using stiffness adaptation analysis (SAA); and
- *Step 4:* Simplified determination of component capacity using well-establish methodologies for "macro-block" analysis of elements.

While each step listed above was studied extensively by previous researchers [e.g., 19, 22, 25, 27, 35, 45, 48], the current research regards an aggregated and comprehensive framework comprising the different state of the art procedures of geometric data acquisition, 3D modeling, and structural analysis in a cohesive, consistent, and efficient fashion. In this regard, the novelty of the paper regards the effectiveness and the continuity across all steps which has not been previously established in the literature in a repeatable way for use by practitioners. The selection of the case study church was based on rational criteria pertaining to its overall risk relative to other churches in the local portfolio, but it's size and components are also representative of a large number of churches, thus making it representative for exhibiting the usefulness of the proposed framework.

2. Step 1: Acquisition of the Geometry of the Church using Photogrammetric Techniques

Photogrammetric techniques are increasingly applied in building surveys to procure geometric information [21, 22, 23]. Geometric information is relevant to the accurate assessment of URM buildings, both for out-of-plane behavior and for global model updating [19, 24, 22, 25]. Given the complex geometry of churches, traditional survey techniques and tools (e.g., triangulation method, total station, and laser scanner) may be inadequate due to inaccessible or visually obstructed church macro-block elements such as the bell tower, nave vaults, or roofs. Therefore, UAS (colloquially referred to as a “drone”) with an on-board high-resolution camera was used to photograph different perspectives of the exterior of the church. Stationary cameras were used for the interior of the church. Subsequently, those photographs were processed using photogrammetric software, resulting in a high-density point cloud in which each point’s position is defined in a three-dimensional reference system. A large number of photographs both outside and inside the building (Figure 2) is required to create a complete 3D model.

Figure 2 – Examples of photographs taken both using UAS and stationary cameras to produce a high-density point cloud.

The photographic acquisition was performed following three best-practice requirements [26]:

- *Completeness*: All exposed surfaces of the entire building were photographed. Any unphotographed “blank” areas could compromise the accuracy of the model and the point cloud density;
- *Overlap*: Adjacent photographs were overlapped for at least 40% of their planar dimensions to capture the same objects with different perspectives, allowing the photogrammetric software to process the photographs with less distortion; and
- *Redundancy*: “Key-points” of the building, such as wall corners or opening vertices were captured in several different photographs in case some of the photographs were discarded for any reason (e.g., blurriness).

A schematic drawing representing the configuration of the photograph acquisition is shown in Figure 3a-b. A *Typhoon H* UAS (Figure 3c) was used during the exterior photogrammetric survey, due to the increased stability under wind provided by the six-rotor configuration and the 360° rotational freedom of the camera. The exterior camera resolution size was 3840 × 2160 pixels with a focal lens length of 35 mm. The photographs were acquired with a lens opening of *f*/2.8 and ISO-100. A digital camera *NIKON COOLPIX L830* (Figure 3d) was used for the stationary interior photographs. The digital camera resolution size was 4608 × 3456 pixels with a focal lens length of 22 mm. The photographs were acquired with a lens opening of *f*/3 and ISO-720.

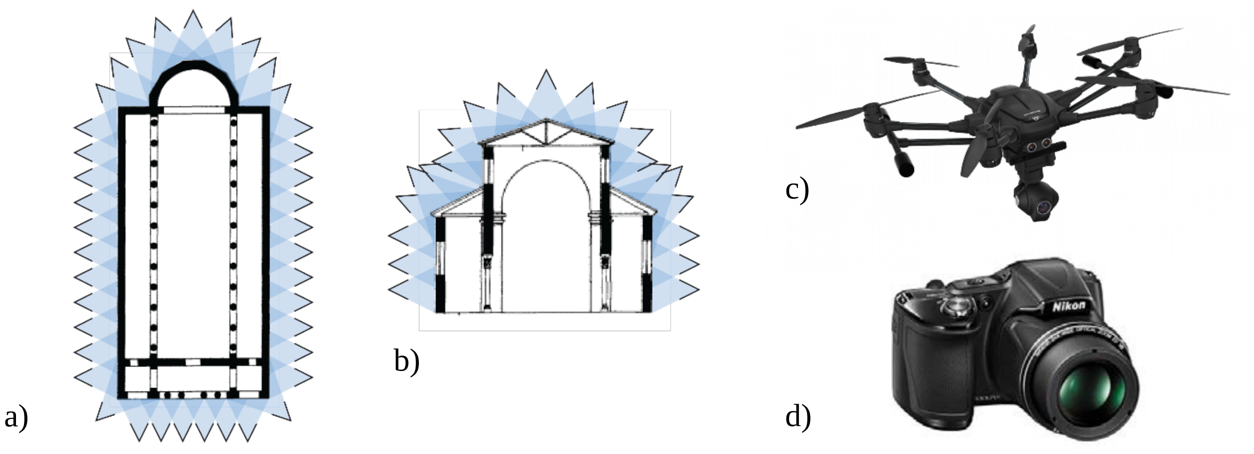

Figure 3 – a) Schematic plan view of the UAS photographic survey; b) schematic elevation of the UAS photographic survey; c) the UAS; and d) the digital camera utilized during the current study.

The photographs were processed using a photogrammetric software (e.g., *Autodesk ReCap Pro®* or *Agisoft Photoscan®*), which utilizes georeferenced meta-data in the photographs to auto-scale the point cloud, thus reducing the post-process time for the scaling of the model. A few measurements of some church components (e.g., doors width and height, façade length, and arches net span) were taken manually to confirm the accuracy of the auto-scaled point cloud from the photogrammetric survey, with an error of approximately 1%. The models produced at the end of the photogrammetric process are shown in Figure 4a (exterior) and Figure 4b (interior) for the case study church.

Figure 4 – High-density point cloud with applied texture of the: a) exterior; and b) interior of the church of Santa Maria Maggiore.

3. Step 2: 3D Modeling of the Church using HBIM

3.1. The HBIM Approach to the seismic risk assessment

HBIM represents both a software tool as well as a holistic approach in the management of the design-related information for a building [27, 28, 29]. A HBIM package for a building may contain not only the 3D geometric shape of the building and its components but also various other data types (e.g., mechanical material properties, structural shell and linear elements, and photographs and worksheets collected during the surveys) that might warrant exchange amongst various designers and facility managers [30]. Thus, "integration" (i.e., integrating in one single model a large amount of multi-source data) and "interoperability" (i.e., comprehensive and bi-lateral interaction with other software) should be considered the key words to apply to the HBIM approach [28]. The information regarding the seismic risk assessment of the church of Santa Maria Maggiore developed by Pirchio, et al. [14] and the mechanical properties of the macro-blocks of the church defined using aggregated non-destructive test techniques (Pirchio, et al. 2020b) were included in the multi-dimensional HBIM-based model as shown in Figure 5. The modeling could be performed with any BIM-based software (e.g., *Autodesk Revit®* or *Graphisoft ArchiCAD®*)

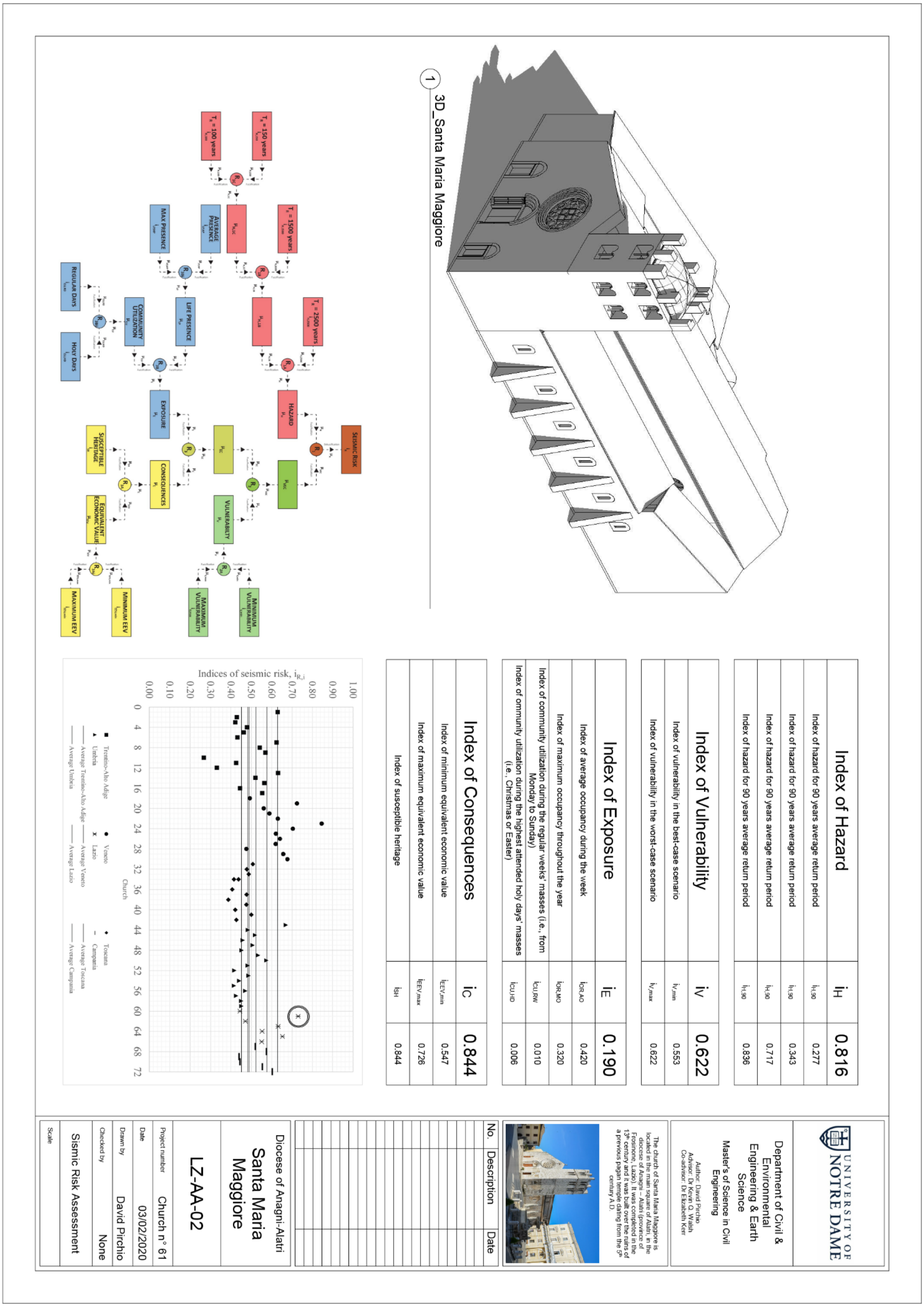

Figure 5 – Overview of the seismic risk assessment of the church of Santa Maria Maggiore.

3.2. The HBIM Approach to the Macro-Blocks Analysis

Due to the height and slenderness of church walls, as well as the poor quality of connections between different URM walls compared to most other types of buildings, subdividing URM churches into units called "macro-blocks" is the preferred method to assess churches and other complex URM buildings [3, 31, 32]. In the Italian seismic assessment guidelines for heritage buildings [33] nine different macro-blocks types are identified for URM churches (Figure 6).

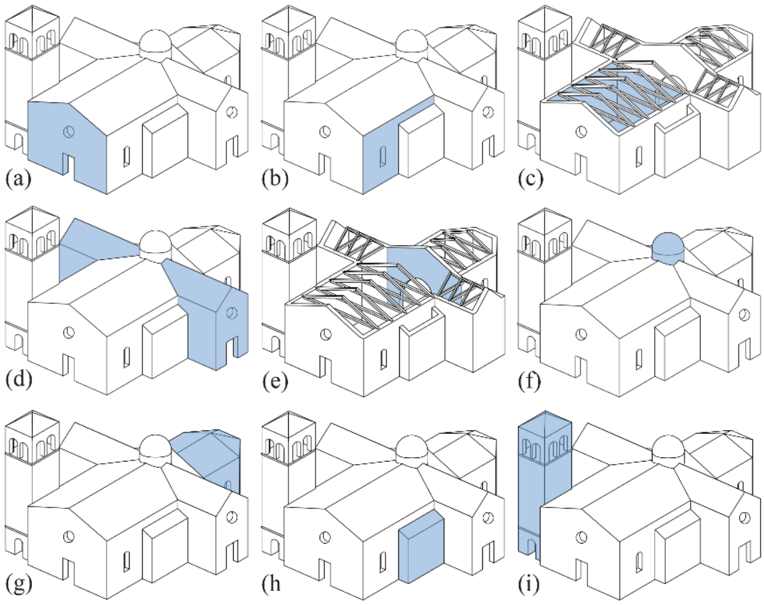

Figure 6 – Macro-blocks considered: (a) façade; (b) lateral walls; (c) naves; (d) transept; (e) triumphal arch; (f) dome; (g) apse; (h) chapels; (i) bell tower.

Each macro-block of the church of Santa Maria Maggiore was identified in the HBIM-based approach, and each single sub-component (e.g., one of the vaults of the macro-block "nave") could be classified and assigned within the HBIM file with particular data regarding the macro-block's material properties and geometry.

Thus, starting from the high-density point clouds developed in step 1, each macro-block was defined and singularly modelled (Figure 7), for use in subsequent analysis of the entire church building.

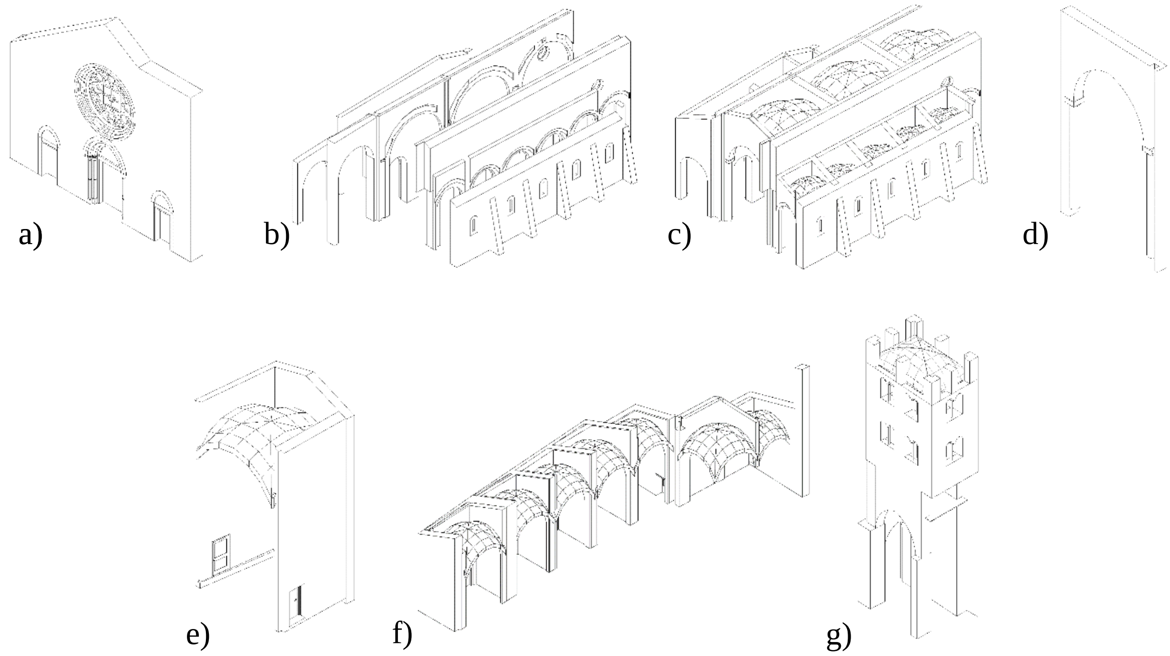

Figure 7 – The macro-blocks of the church of Santa Maria Maggiore: a) façade; b) lateral walls; c) naves; d) triumphal arch; e) apse; f) chapels; g) bell tower.

4. Step 3: Structural Analysis of the Church using FEM Analysis

Simplified analysis techniques (e.g., linear equivalent static or modal response spectrum) and FEM analysis are not suitable for particularly complex URM buildings (such as churches) due to the discontinuity and non-homogeneity of the URM [34]. Alternative structural modeling approaches based on finite-discrete elements (FDE) and discrete elements (DE) were proposed by different authors [35, 36, 37, 38]. However, these alternative approaches require a niche expertise as well as specific software that is not common to the industry at large.

Given the practice limitations of highly specialized analysis, the current research shared the aim of other authors [39, 40] to explore the possibilities of FEM analysis and modal response spectrum analysis to approximate reasonable results for complex URM structures like the selected case study church. Shell elements were chosen for the FEM analysis – as opposed to solid elements – to maintain a direct interconnection between the geometric 3D model and the finite element model, because only shell elements could be directly exported from the HBIM-based software into the FEM software.

Finite-discrete element models (FDEM) and discrete element models (DEM) with discrete, solid elements representing the masonry units have been shown to provide more precise behavior of URM buildings than do shell elements in a FEM [34]. However, a shell-element-based FEM offers non-negligible advantages in modeling, both in terms of cost-efficiency and in terms of replicability of the procedure for practicing engineers, and it still provide accurate results [41]. Furthermore, some of the limitations of the shell element modeling can be overcome by using the model as a starting point for the macro-block analysis and by performing a stiffness adaptation analysis (SAA), both of which were considered in the current study and described hereafter.

4.1. The HBIM Approach to the FEM Analysis

In addition to being a useful storage of information regarding the composing material, the macro-blocks, and the provisional regional-scale qualitative seismic risk assessment of the case study church, the developed HBIM-based model (Figure 8a) was also implemented as a base for a FEM of the church. Consistent with the principle of interoperability" [30, 28], the model also contains structural information regarding the approximated shell elements representing the walls and the vaults of the church (Figure 8b).

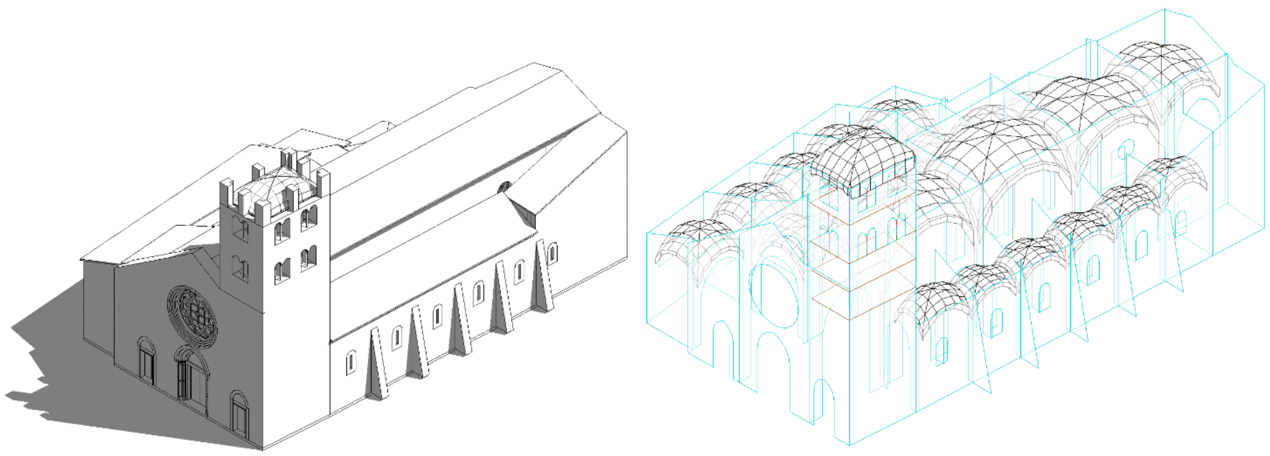

Figure 8 – a) Geometric HBIM-based model; and b) structural HBIM-based shell elements model of the church of Santa Maria Maggiore.

The shell elements for the model were directly exported to the FEM software through the .ifc file [30] with limited data-loss regarding the modeled macro-blocks (e.g., a few shell elements could not be exported due to their significant geometric complexity). To obtain a correct exportation of the vaults during the HBIM modeling, a parametric approximation of flat 4-node surfaces was utilized (Figure 8).

4.2. Design Response Spectra

The response spectrum analysis was performed assuming a 710-year median return period to address the largest resulting stresses and the dominate modal shapes (in terms of participating mass) for each macro-block, as a necessary premise to any retrofitting intervention proposal. The resulting seismic inertial forces were combined using Equation 1 – 2 provided by the Italian Technical Standard for Constructions [42] and its commentary [43]:

$$1.00E_x + 0.30E_y \tag{1}$$

$$0.30E_x + 1.00E_y \tag{2}$$

where: E_x and E_y are the resulting seismic inertial forces in x and y building plan principal directions.

Variable		**Value**
Reference period in which the earthquake might happen	V_R [years]	75
Probability of exceedance of the considered earthquake intensity within the reference period	P_{V_R} [%]	10
Soil category	-	A
Topographic category	-	T1
Peak ground acceleration	a_g [g]	0.2687
Magnification factor	F_0	2.5206
Corner period	$T_C{}^*$ [s]	0.3616
Behavior factor for horizontal accelerations (corresponding to the *R* factor in the ASCE 7)	q_h	2

Table 1 – Assumptions to determine the elastic and design response spectra according to MIT [42, 43].

The elastic and design response spectra were determined accordingly with the MIT [42] using the assumptions in Table 1, and they are shown in Figure 9. Please note that the corresponding acceleration at the plateau of the elastic response spectrum for the 1-in-500 years earthquake, S_{DS}, would correspond to a moderate level of seismicity according to the American Standards [44], since $0.33g < S_{DS} = 0.41 < 0.50\ g$.

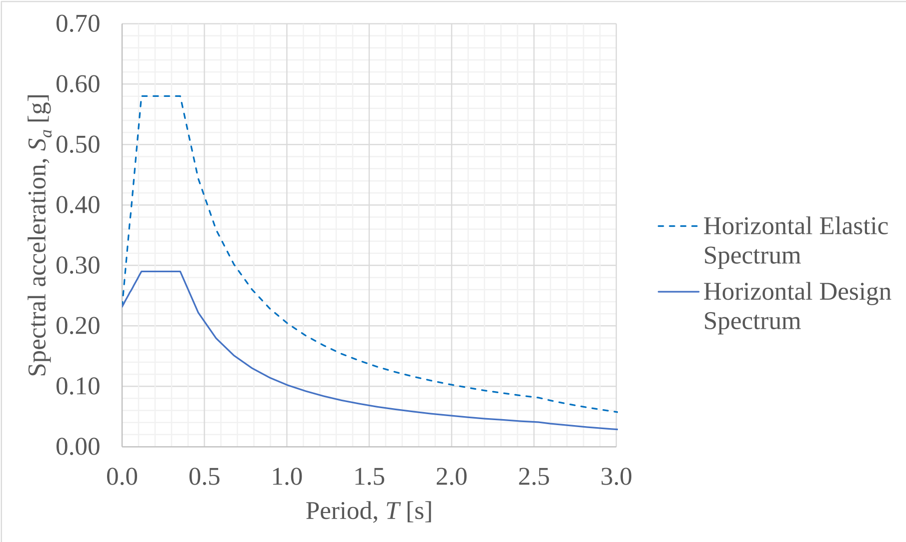

Figure 9 – Horizontal elastic and design response spectra.

4.3. Structural analysis

4.3.1. The FEM Model

The HBIM-based model was exported into *CSi SAP2000®*, and the FEM model is shown in Figure 10. The walls were initially modeled as shell elements fully "fixed" (i.e., translationally and rotationally restrained in all three axes) at the base. The masonry piers were initially modeled with rotational restraints at the top and bottom. A rotationally restrained connection between perpendicular walls was assumed as well. The masonry columns were modeled as frame elements assumed as hinged both at the top and at the bottom. The masonry vaults were modelled consistently with their geometric imperfections such that the edges were not perfectly coincident with the centerlines of the walls. Thus, translationally rigid connectors were added to link the vaults and the walls. Nonetheless, the rotation of the vault edges around their weak axis was allowed. Given that it was not possible to survey the roof and the reinforced concrete bond beam sitting on top of the walls, the connection between the roof and the top of the walls was conservatively assumed to be poor, consistent with observation in late 20th century following retrofitting interventions [45, 46]. Thus, the roof was modelled only as an additional dead load and assumed to provide no diaphragm action. The latter choice was conservative since because of the lack of diaphragm action, the walls would respond to the seismic excitation more similarly to cantilever systems (the response would still not be completely independent given the wall-to-wall connections). Furthermore, considering the roof as a dead load resulted in larger seismic demand and allowed to still capture the compression on top of the walls, which play a key role when determining the shear and rocking strength of URM walls.

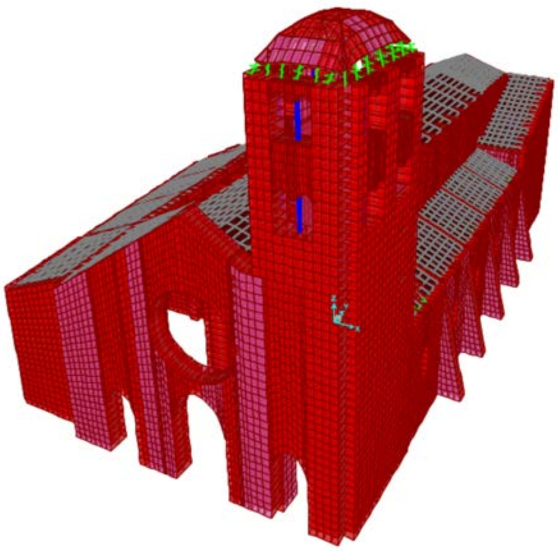

Figure 10 – FEM model of the church of Santa Maria Maggiore.

The sum of the resulting shear stresses, τ_{21} and τ_{23} in Figure 11 (σ_{33} is assumed equal to zero in the structural analysis model), was checked against the frictional shear capacity of the wall determined accordingly with the Mohr-Coulomb theory [47] in Equation 3:

$$\tau_{21} + \tau_{23} \leq f_{vn} = c + \mu\sigma_{22} \tag{3}$$

where: f_{vn} is the shear capacity of the URM;

c is the cohesion of the URM;

μ is the coefficient of friction of the URM;

σ_{22} is the compressive stress acting at the considered section of the wall.

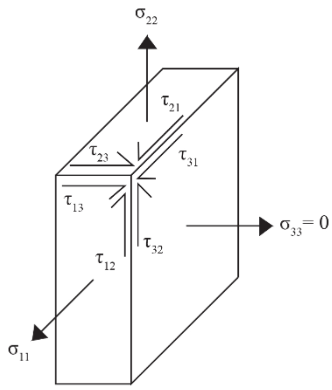

Figure 11 – Positive direction of the stresses on a typical wall shell element.

Both sides of the connection were controlled (i.e., the two edges of the connected perpendicular walls). If the condition expressed in Equation 3 was satisfied, then the fixed connection between the connected walls was retained in the model. Otherwise, horizontal translational releases were applied to the connection in the out-of-plane direction of the wall as well as rotational releases with respect of the out-of-plane rotation. The condition provided by Equation 4 was checked iteratively until all the wall-to-wall connections and the wall-base restraint shear demands satisfied the shear friction capacity. Note that residual friction capacity was neglected in the analysis.

In Table 2 the mechanical material properties of each macroblock of the case study church are shown. The material properties were determined by Pirchio, et al. [18].

Macroblock	**Compressive strength, f'_m [MPa]**	**Young's modulus, E_m [MPa]**	**Shear modulus, G_m [MPa]**	**Cohesion, c [MPa]**	**Coefficient of friction, μ**	**Density, γ [kN/m^3]**
Façade	8.13	3258	995	0.102	0.722	22
Lateral Walls	3.77	1608	502	0.073	0.563	21
Naves	5.54	2218	678	0.109	0.768	22
Triumphal Arch	6.96	2787	851	0.109	0.768	22
Roofs	25 kN/m^3 specific weight concrete was assumed for determining the dead load					
Apse	3.77[1]	1608[1]	502[1]	0.073[1]	0.563[1]	21
Chapels	3.77[1]	1608[1]	502[1]	0.073[1]	0.563[1]	21
Bell Tower	6.80	2724	832	0.102	0.722	22

[1]Since no measurements were taken at these locations, the worst material properties measured in other locations on the case study church were assumed.

Table 2 – Mechanical material properties assumed for the analysis.

4.3.2. Dynamic Properties and Stress Status of the Structure

A modal analysis was performed on the FEM model of the case study both for the initial condition (i.e., fixed wall-to-wall connections) and for the final condition (following the end of the process of iteratively releasing the connections). Sixteen modes were analyzed to achieve at least 70% of participating mass in *x* and *y* direction. The first eight mode shapes are shown both for the initial and final conditions (Figure 12 and Figure 13). The periods of vibration and the corresponding participating masses for each of these modes are shown in Table 3.

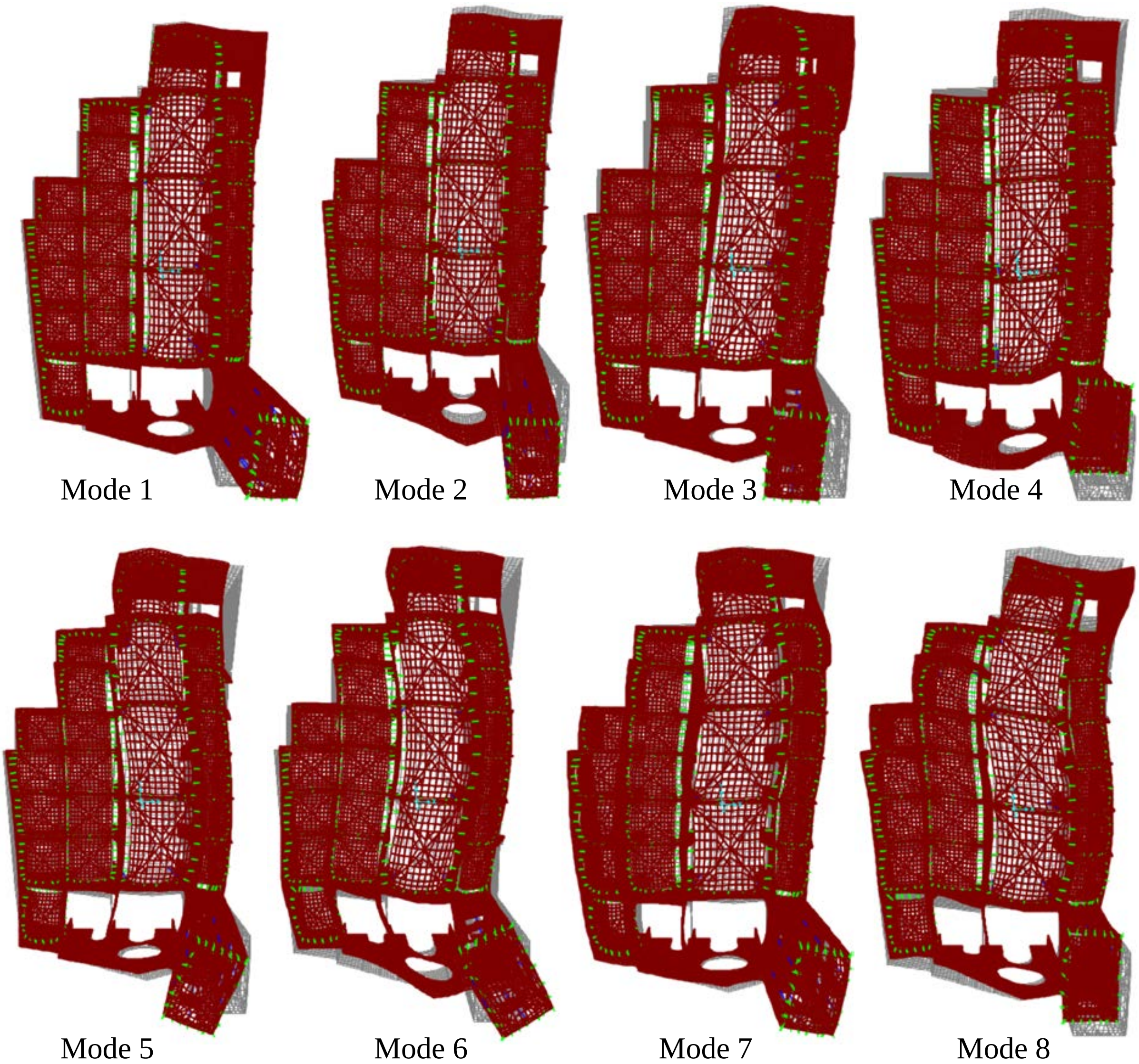

Figure 12 – First eight mode shapes for the initial condition.

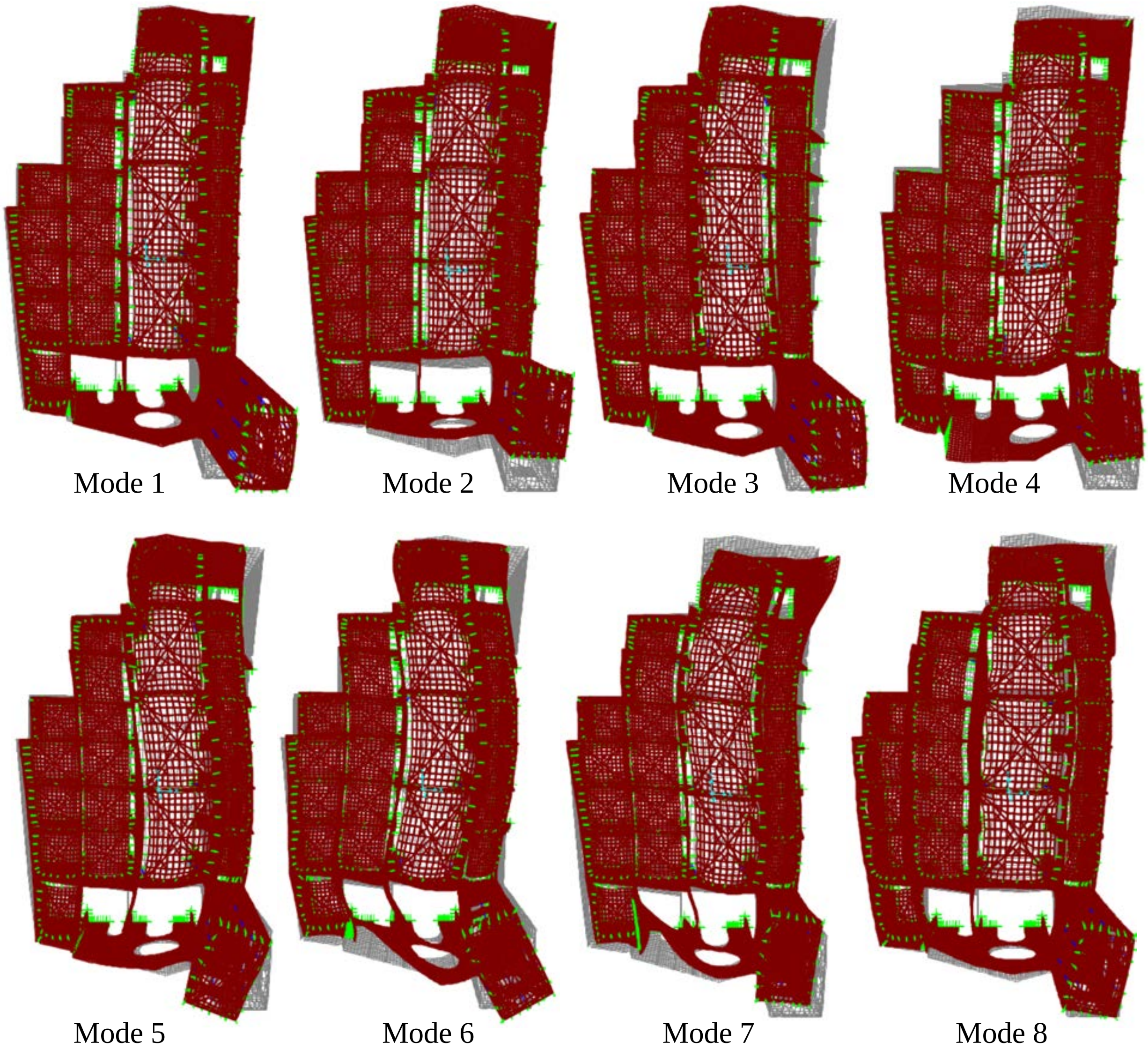

Figure 13 – First eight mode shapes for the final condition.

Condition	Dynamic property	Mode 1	Mode 2	Mode 3	Mode 4	Mode 5	Mode 6	Mode 7	Mode 8
Initial	Period, T [s]	0.234	0.205	0.194	0.154	0.151	0.123	0.111	0.110
	Participating mass, U_x [%]	48.85	3.36	13.22	0.26	0.15	0.10	6.98	0.02
	Participating mass, U_y [%]	2.23	46.44	0.02	18.83	2.34	1.61	0.01	0.13
Final	Period, T [s]	0.239	0.205	0.196	0.157	0.153	0.125	0.114	0.111
	Participating mass, U_x [%]	45.25	3.88	16.62	0.35	0.02	0.20	1.26	5.50
	Participating mass, U_y [%]	2.55	47.06	0.09	18.32	0.06	0.66	2.18	0.16

Table 3 – Dynamic properties of the first eight mode shapes for both the initial and the final conditions.

As can be observed in Figure 12 and Figure 13, the first two modes (which involve the largest participating mass) are dominated by the vibration of the bell tower and the façade. Furthermore, modes 1, 3, and 7 together contribute approximately 75% of participating mass in the x-direction, while modes 2, 4, and 5 together contribute approximately 70% of participating mass in the y-direction (Table 3). Although the rotational-translational releases applied to the wall-to-wall and wall-to-base connections slightly affected the dynamic behavior of the building (Table 3), the differences were almost negligible. In fact, although the new restraints are much less stiff, only a few wall-to-wall connections experienced a shear and moment failure and mainly on the façade and bell tower. Therefore, the global behavior represented in Table 3 resulted lightly affected and only small increase of the period was experienced. More differences might be noticed in modal shape mainly involving the façade and bell tower (i.e., modes 2, 6, 7, and 8) when comparing Figure 12 and Figure 13.

Subsequently, a modal response spectrum analysis was performed to compute the design demands associated with the 1-in-710 years earthquake. The compressive stresses and the shear stresses (both in-plane and out-of-plane) were determined to identify critical zones of stress concentration. In general, the compressive stresses determined in the worst-case scenario (Figure 14a) were smaller than the compressive capacity of the URM material (Table 2). Nonetheless, the piers of the façade and of the bell tower were found to be subjected to large shear stresses (Figure 14b, c, and d), and thus, these macro-block elements were analysed in greater detail, as discussed in the next section.

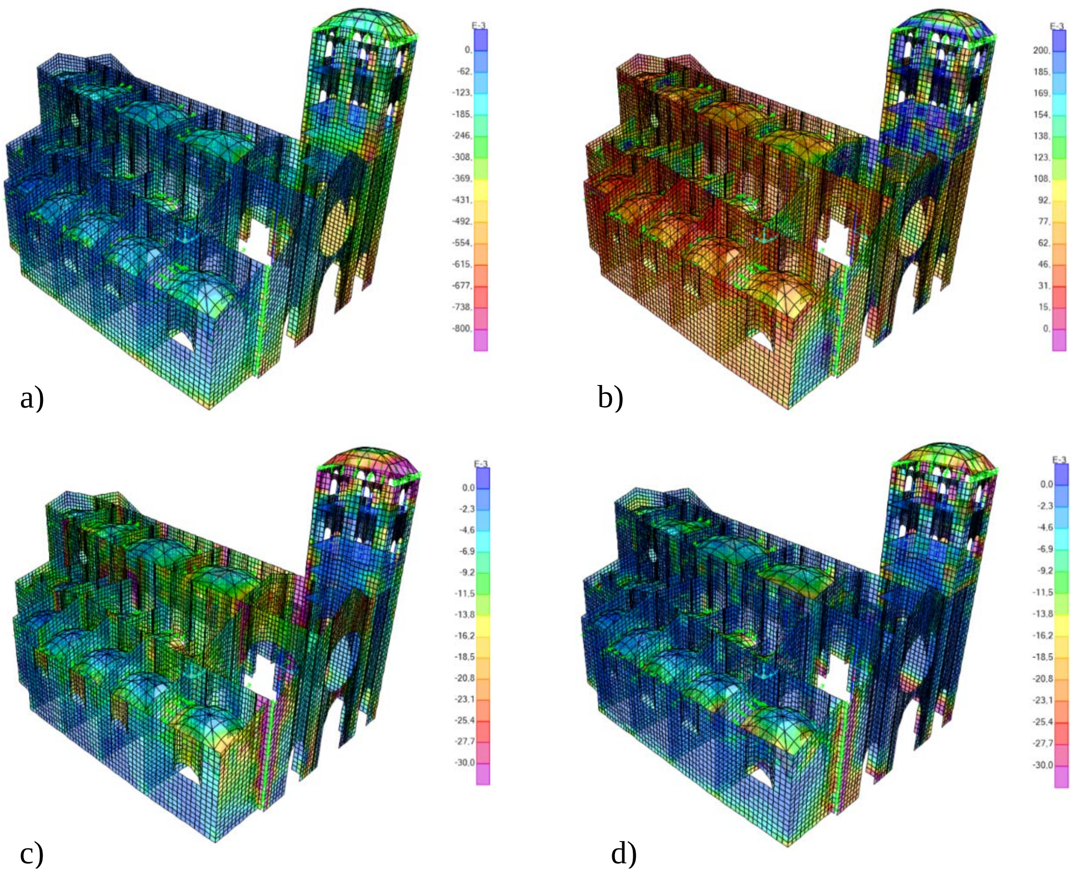

Figure 14 – Stress: a) σ_{22}; b) τ_{12}; c) τ_{13}; d) τ_{23}. Please note that the units in Figure 14 are in MPa and that the stress directions are in accordance with Figure 11.

Although the FEM analysis adopted herein is not suitable to simulate the actual failure mechanisms of the macro-blocks, in the current research it was used (given its wide practitioner acceptance) to determine the resulting stresses that can be used to identify where crack lines governing macro-block formation would most-likely develop. The most likely crack lines of the gable mechanism on the façade were identified using the FEM (Figure 15) and assessed via the virtual works approach as discussed in the next section.

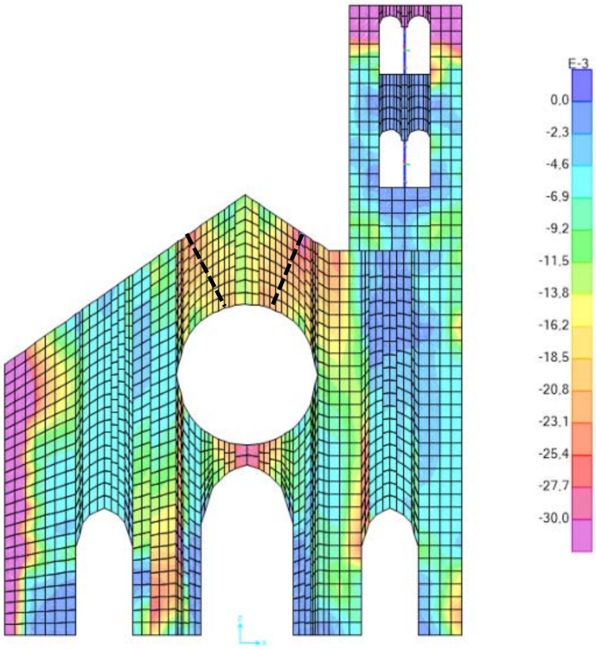

Figure 15 – Out-of-plane shear stresses on the façade with likely crack lines for the gable mechanism identified.

5. Step 4: Local Macro-blocks Failure Mechanisms

Although the analysis of local macro-blocks failure mechanisms underwent major advancements in the last decade via use of NURBS-based software and sequential linear programming of adaptive mesh [48, 49, 50, 51], the knowledge and the tools to perform this type of advanced analysis are still not available to the wide audience of practitioners which currently populate the world of engineering.

The aim of the current section was to show how procedure developed so far can be used as a aid for the traditional macro-blocks analysis in terms of selection of the relevant local failure mechanisms and identification of the most likely crack lines (Figure 14, and Figure 15). Therefore, the the pier mechanisms of the bell tower and on the gable mechanism of the façade were analyzed herein a possible example.

5.1. Pier Mechanism

URM piers should be checked against three mechanisms: rocking and toe crushing, diagonal shear, and sliding shear [52, 53, 54, 42] resulting in Equation 4 – 6.

$$V_{rocking} = \frac{Dt\sigma_0}{2\psi\frac{H}{D\,(or\,t)}}\left(1 - \frac{\sigma_{22}}{0.85f'_m}\right) \tag{4}$$

$$V_{diagonal} = \frac{Dt}{b} f_{ut} \sqrt{1 + \frac{\sigma_{22}}{f_{ut}}} \tag{5}$$

$$V_{sliding,in-plane} = Dt f_{ut} \tag{6}$$

where: D is the depth of the URM pier;

t is the thickness of the URM pier;

H is the height of the URM pier;

ψ is a coefficient equal to 1.0 for cantilever piers and 0.5 for fixed-fixed piers;

f_{ut} is the tensile strength of URM, $f_{ut} = c + \mu\sigma_{22}$;

b is the shear stress distribution factor, with $1 \leq b = H/D \leq 1.5$

The FEM model might be used to determine the forces and the moments acting at the base and at the top of each URM pier in order to perform a demand versus capacity check. As an example, the capacity of the piers of the façade and the bell tower were checked against the force demand obtained by the modal response spectrum analysis. The results are shown in Figure 16.

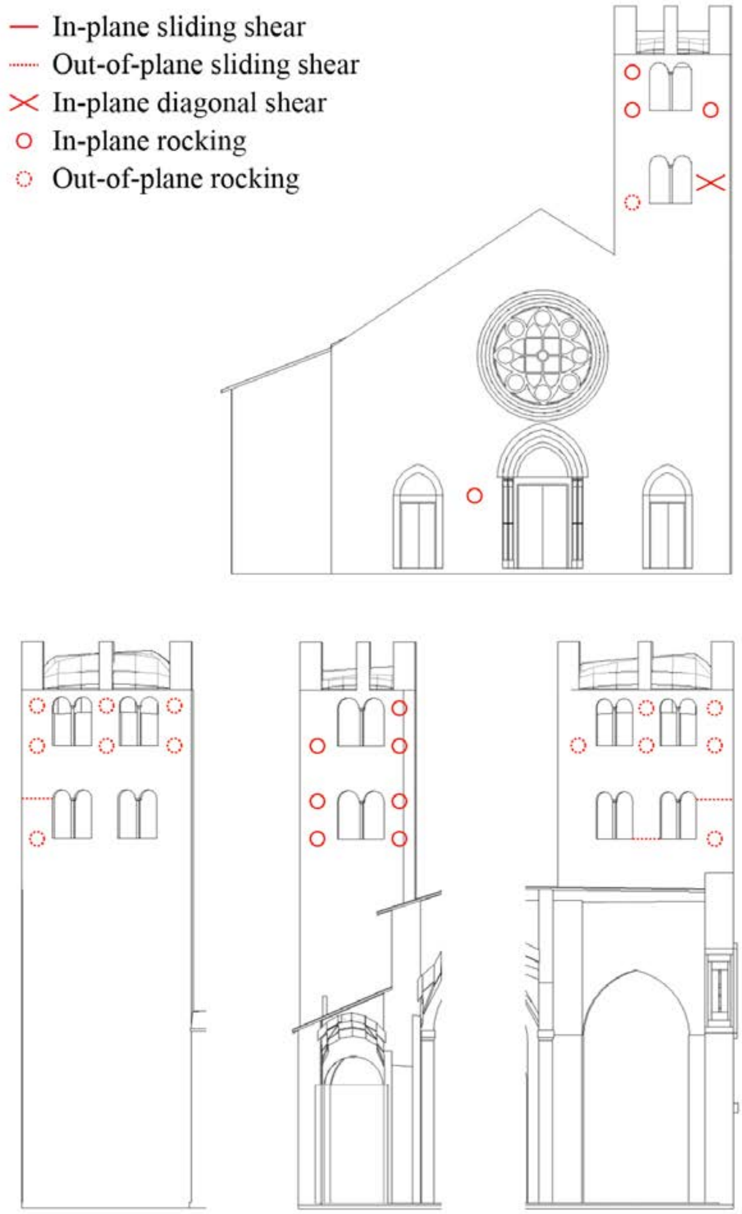

Figure 16 – Failure mechanisms of the piers of the façade and of the bell tower.

5.2. Gable Mechanism

The gable mechanism is identified as one on the most affecting macro-blocks failure mechanism for the façade [33]. Due to the rose-window (i.e., the large circular opening on the façade), the gable of the façade of the church of Santa Maria Maggiore is subjected to significant out-of-plane forces which might likely lead to the out-of-plane collapse of the gable (Figure 17, Figure 18a and b).

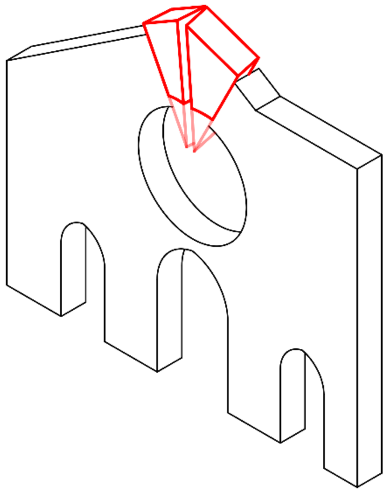

Figure 17 – Schematic representation of the gable mechanism.

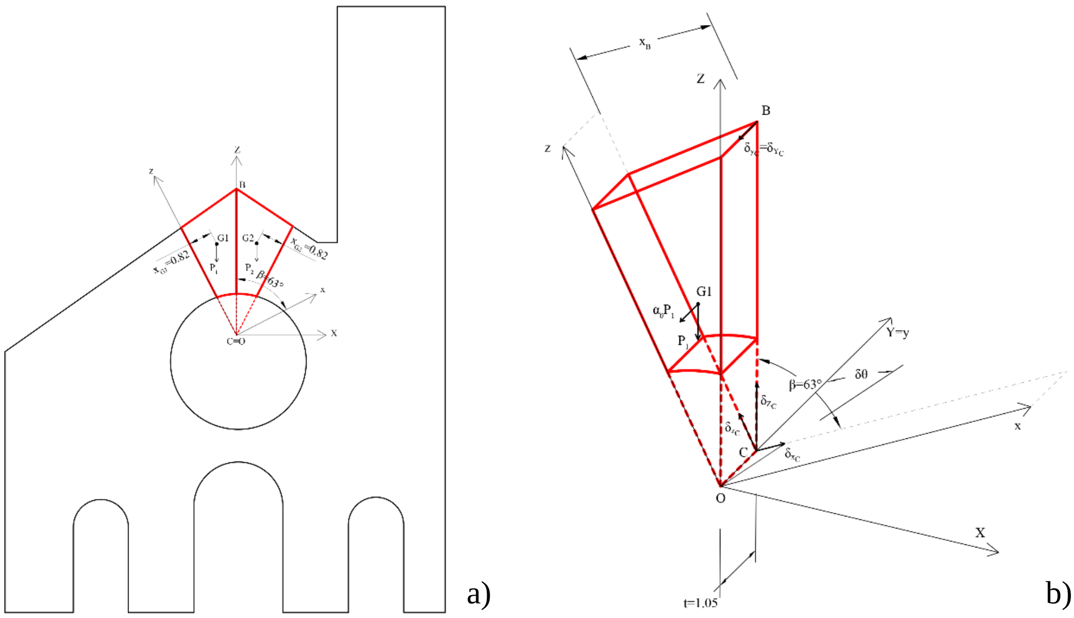

Figure 18 – a) elevation of the gable mechanism; b) isometric representation of one of the rigid blocks and relative displacements. Units of m.

To determine if the gable might collapse under the inertial forces imposed by the considered design response spectrum (Figure 9), the linear kinematic approach was used [55], which is a type of analysis based on the virtual work principle. The horizontal inertial forces acting on the gable are considered equal to the self-weight multiplied by an inertial multiplier α_0, as shown in Figure 18b (in which one single block is shown considering the second one symmetric). Considering the two blocks composing the mechanism as rigid (Figure 17), the sum of work produced by the inertial forces and the work produced by the self-weights of the rigid blocks was equated to zero in Equation 7 [55]:

$$\alpha_0\left(\sum_{i=1}^{2} P_i \cdot \delta_{Y,P_i}\right) - \sum_{i=1}^{2} P_i \cdot \delta_{Z,P_i} = 0 \quad (7)$$

where: P_i is the self-weight of the i-*th* block;

δ_{Y,P_i} is the translation along the Y-axis of the center of gravity of the i-*th* block;

δ_{Z,P_i} is the translation along the Z-axis of the center of gravity of the i-*th* block.

The inertial multiplier, α_0, necessary to develop the mechanism can be determined using Equation 8 [55].

$$\alpha_0 = \frac{(P_1+P_2)\left[\frac{t}{2}\cos\beta + t\tan\beta\sin\beta\right]\delta\vartheta}{(P_1 x_{G1} + P_2 x_{G2})\delta\vartheta} \quad (8)$$

In general, given that the position and the inclination of the yield lines would be unknown, Equation 8 would have too many variables (i.e., α_0, β, and x_{G1}=x_{G2}) and a relatively complex optimization problem would be required to determine the minimum value of α_0. However, thanks to the FEM analysis, the most likely configuration of the yield lines was determined already (Figure 15), thus, the value of the inertial multiplier can be easily determined to be $\alpha_0 = 1.26$.

6. Validation of the Findings by applying a Pushover Analysis via Stiffness Adaptation

To confirm the results and the observations obtained via the simplified response spectrum analysis, an enhanced non-linear static analysis (i.e., non-linear pushover analysis) was performed in the structural model. Non-linear stress-strain analysis for URM buildings is sometimes carried out in highly specialized software [56, 57, 58], but with the goal of providing an accurate means of replicating the precision and accuracy of results from highly specialized software but in FEM tools more commonly used in practice, the traditional non-linear pushover analysis was enhanced into a multi-step pushover method called a “stiffness adaptation analysis” (SAA) [59].

The SAA consists of an iterative linear pushover analysis in which at the end of each step the shell elements that experienced tensile stresses or exceeded the compressive strength of the material are removed. Thus, the result of the iterative SAA process is equivalent to performing multiple non-linear pushover analyses but with the initial stiffness being degraded at each iterative step. A graphic representation of different steps is shown in Figure 19 and 20, while the algorithm applied in the iterative process was described in Figure 21.

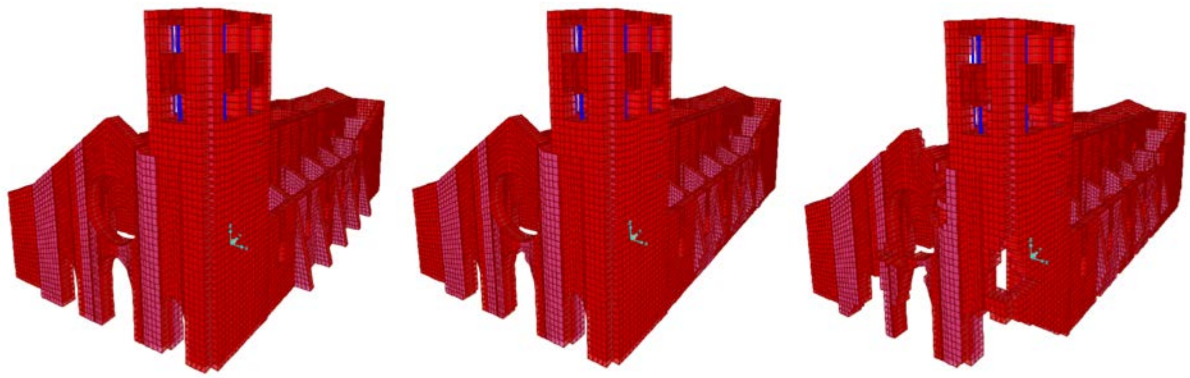

Figure 19 – SAA in N-S direction.

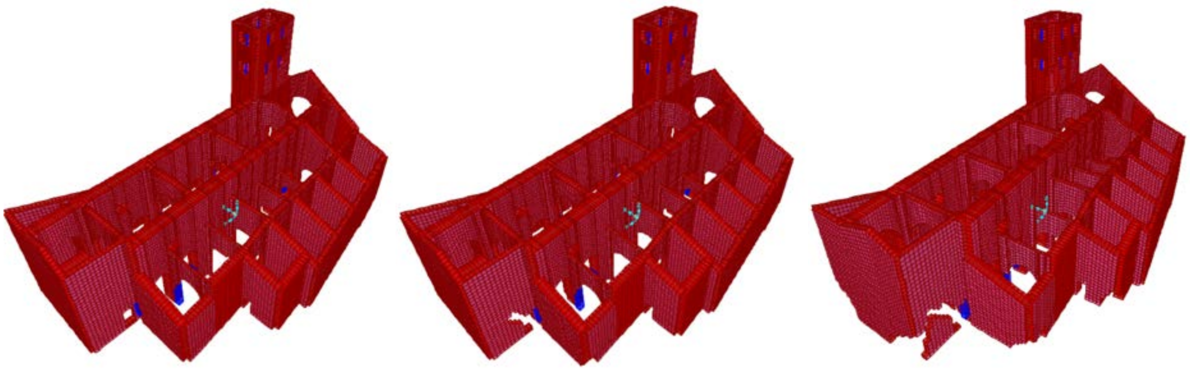

Figure 20 – SAA in E-W direction.

Although the SAA can be used to accurately represent URM component behavior and to ensure numerical convergence in the model, it still presents some limitations as follows:

- As for the traditional non-linear pushover analysis, out-of-plane behavior is disregarded;
- The SAA has a high computational demand since the multiple iterations require running the model multiple times;

- The SAA is sensitive to the selected displacement increment, Δ_{i+1} (Figure 21), as smaller intervals would result in more accurate results but also in extended computational times; therefore, a careful calibration of Δ_{i+1} is required;
- The identification and removal of the shell elements in the model which exceeded the compressive or the tensile material capacity may be need to be done manually pending the development of a separate program to automate this process; and
- Since some elements are removed from the model at each step of the iterative process, SAA is not suitable for cyclic analysis.

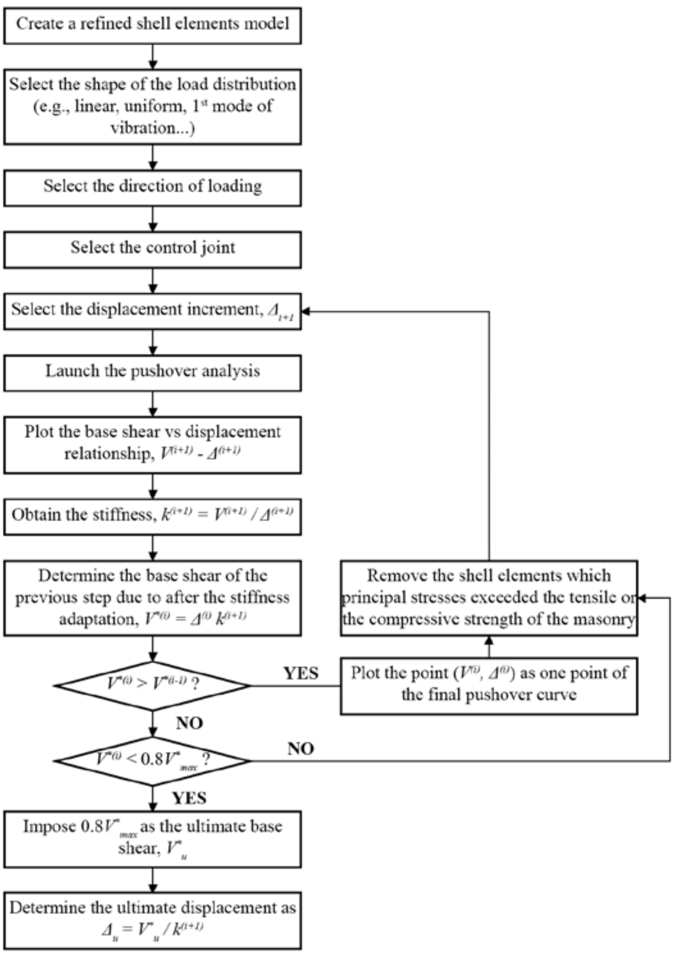

Figure 21 – Algorithm of the SAA iterative process.

Thus, the pushover capacity curves in North-South and East-West directions (respectively *x* and *y* in the model) were determined for the multi-degree of freedom (MDoF) model as shown in Figure 23. The loads were distributed proportionally to the fundamental mode in the direction under consideration (i.e., a triangular load pattern). Given the representative nature of the study case, no other load patterns were considered as further analysis would have exceeded the scope of the research.

Note that the displacement was expressed in terms of drift ratio of the selected control point (Figure 22). Since a global analysis was performed, the control point was selected as close to the center of gravity of the roof level as possible and at the intersection of two bearing walls of the structure so that the increased stiffness given by the return wall prevented the local deformation of the wall to significantly affect the results. Please note that the SAA, as well as the traditional non-linear pushover analysis, is sensitive to the selection of the control point. Local SAA of single macro-blocks could be performed as well by selecting the localized control point accordingly.

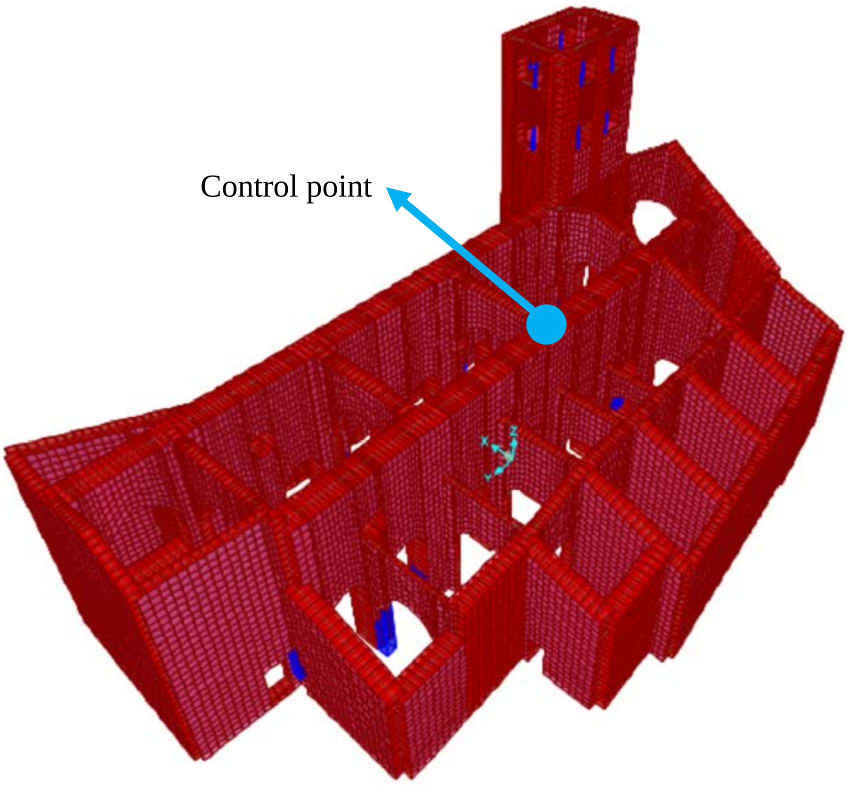

Figure 22 – Selected control point for the pushover analysis.

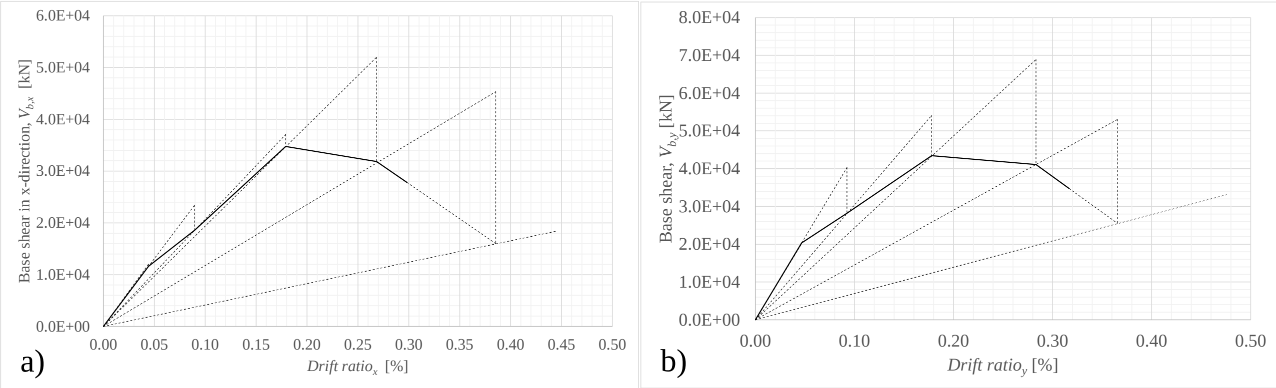

Figure 23 – Capacity curves for the MDoF system: a) N-S direction (x); b) E-W direction (y).

For comparison with the demand spectrum, an equivalent single degree of freedom (SDoF) capacity curve was derived from the MDoF curve. The equivalent SDoF curve was obtained per the provisions of MIT [43] by scaling both the coordinates (*Drift ratio$_i$*) and the ordinates (base shear, $V_{b,i}$) of the original curve using the sum of modal participation factors of the first eight modes, $\Sigma\Gamma_i$, as described in Equation 9. Only the modal participation factor of the first mode would typically be used to scale the MDoF curve into a SDoF curve; however, previous studies showed that this simplification is inadequate to capture the often significant effects of higher modes for complex structures [60].

$$\begin{cases} Drift\ ratio_i^{(SDoF)} = Drift\ ratio_i^{(MDoF)} \Big/ \sum \Gamma_i \\ V_{b,i}^{(SDoF)} = V_{b,i}^{(MDoF)} \Big/ \sum \Gamma_i \end{cases} \tag{9}$$

where: Γ is the modal participation factor as defined in Equation 10.

$$\Gamma_i = \frac{\varphi^T{}_i M \tau}{\varphi^T{}_i M \varphi_i} \tag{10}$$

where: φ_i is the vector of the modal *i*-th mode of vibration;

M is mass matrix of the structure;

τ is the influence vector corresponding to the direction of loading.

In Figure 24 the equivalent capacity curve relative to the SDoF system was shown.

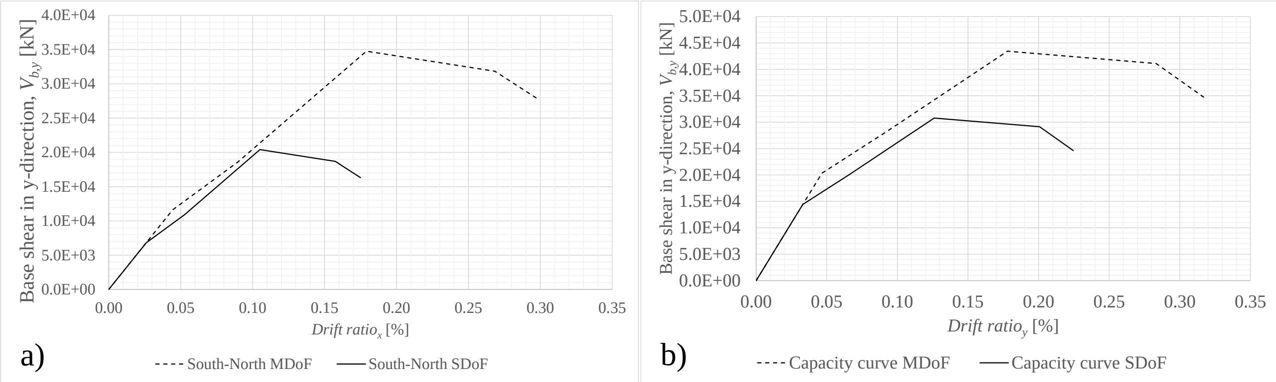

Figure 24 – Capacity curves for the SDoF system: a) in N-S direction (x); b) in E-W direction (y).

Once the capacity curve for the SDoF system was obtained, the performance point (PP) for all the limit states (i.e., immediate occupancy, damage limitation, life safety, and collapse prevention) was determined comparing the capacity curve with the corresponding demand spectrum. The comparison was based on an iterative process in order to find the equivalent damping ratio, ξ_{eq}, to be used for each limit state to scale the demand spectrum. MIT [43] proposed Equation 11 to determine ξ_{eq}, and the iterative process to obtain the PP is charted in Figure 25.

$$\xi_{eq}{}^{(i+1)} = k\,\frac{63.7\left(F_y{}^{*(i)} d_{PP}{}^{*(i)} - F_{PP}{}^{*(i)} d_y{}^{*(i)}\right)}{F_{PP}{}^{*(i)} d_{PP}{}^{*(i)}} + 5 \tag{11}$$

where: $\xi_{eq}{}^{(i+1)}$ is the equivalent damping ratio (percentage) to be used in the *i*+1-th step;

$F_y{}^{*(i)}$ and $d_y{}^{*(i)}$ are the coordinates of the equivalent yielding point of the bilinear curve;

$F_{PP}{}^{*(i)}$ and $d_{PP}{}^{*(i)}$ are the coordinates of the equivalent PP of the bilinear curve;

k is 0.33 for structures with low dissipation capacity.

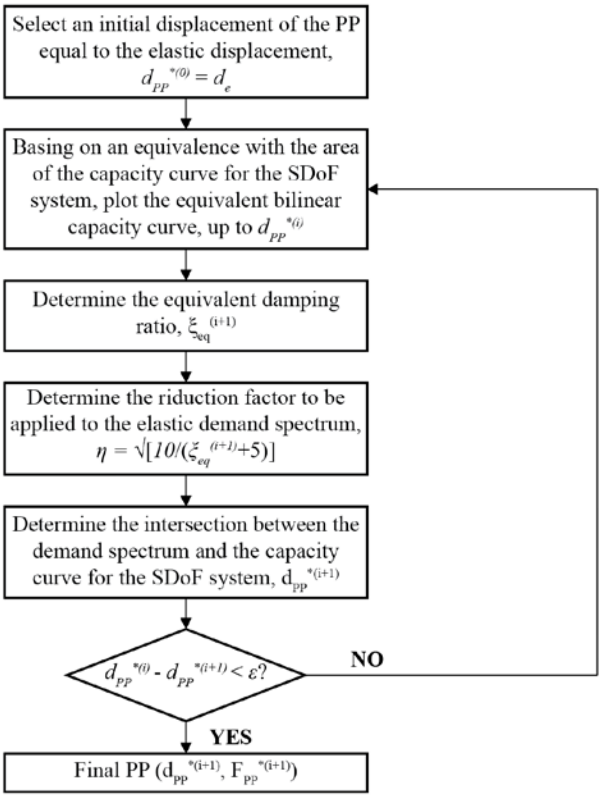

Figure 25 – Algorithm for the iterative process to determine the PP, according to MIT [43].

Applying the procedure shown in Figure 25 for each limit state resulted in the PPs indicated in Figure 26. It might be noticed that the poorest performance corresponded to an earthquake excitation in North-South direction (Figure 26a). In the East-West direction, the capacity largely exceeded the demand (Figure 26b) most likely due to the substantially proportioned resisting walls oriented in the East-West direction. Furthermore, focusing on Figure 20, it might be noticed that, according to the analysis, the damage was concentrated on the façade and the bell tower. This observation is consistent with the results of the modal analysis (Figure 13) and the response spectrum analysis (Figure 14, Figure 15, and Figure 16).

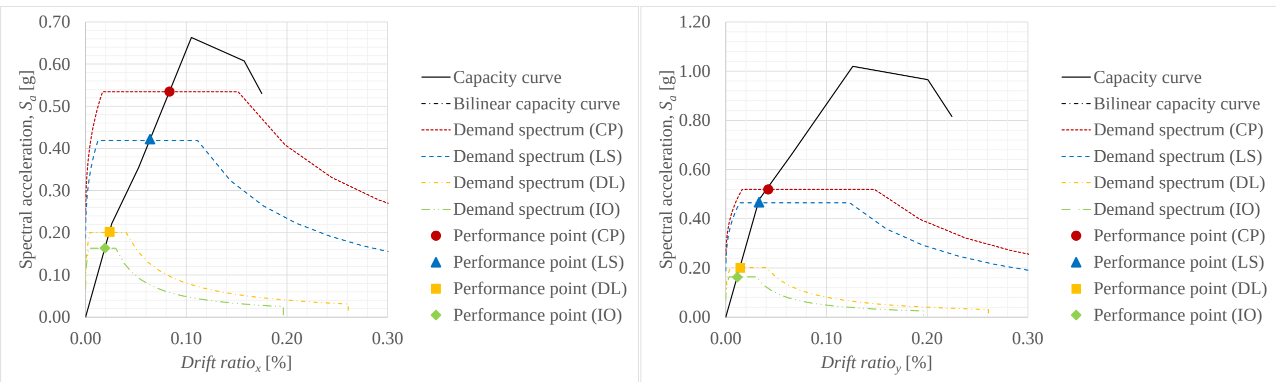

Figure 26 – a) Performance point (PP) in N-S direction (x); b) PP in E-W direction (y).

The equivalent damping ratio, ξ_{eq} , the reduction factor to be applied to the elastic demand spectrum, η, and the behavior factor for horizontal acceleration (corresponding to the *R* factor in ASCE 7), q_h, related with each PP are listed in Table 4. Please note that, although they have different definitions, the factor η and the coefficient q_h are applied for the same purpose and with the same physical meaning (i.e., reducing the demand spectrum due to the capability of dissipating energy of the structure), and they can be considered as reciprocal values in the equations proposed by MIT [42]. Note that the maximum response spectrum modification factor, q_h, resulting from the pushover SAA was smaller than the one assumed in the response spectrum analysis as suggested by MIT [42] in general for URM buildings.

Considered direction	Limit state considered for the PP	Equivalent damping ratio, ξ_{eq} [%]	Reduction factor, η	Response spectrum modification coefficient for horizontal acceleration, q_h
North-South	Immediate occupancy, IO	5.00	1.00	1.00
	Damage limitation, DL	5.00	1.00	1.00
	Life Safety, LS	7.29	0.90	1.11
	Collapse prevention, CP	6.98	0.91	1.09
East-West	Immediate occupancy, IO	5.00	1.00	1.00
	Damage limitation, DL	5.00	1.00	1.00
	Life Safety, LS	5.00	1.00	1.00
	Collapse prevention, CP	7.47	0.90	1.12

Table 4 – Equivalent damping ratios and reduction factors related with the structure performance points.

The pushover analysis via SAA was applied in order to model the global behavior of the church, but the authors wish to highlight the possibility of this application also for addressing the failure mechanisms of single macro-blocks by selecting appropriate control point [61]. As the global SAA pushover was used to validate the response spectrum analysis, the local pushover SAA might be used as a validation for the kinematic analysis shown in Figure 17 and Figure 18.

7. Summary and Conclusion

A four-step framework was developed and applied to the case study of the URM church of Santa Maria Maggiore in the diocese of Anagni-Alatri (Lazio, Italy) to acquire the necessary geometric dimensions in form of a high-density point cloud (1), to convert the point cloud into a solid 3D HBIM-based model attached with data regarding the material properties and the structural elements (2), and to export the latter into FEM software to perform a modal response spectrum analysis, a local collapse mechanisms analysis, and a SAA(3).

Beneficial features of the proposed framework could be identified for each step as follows:

- *Step 1*: The use of UAS and stationary cameras to perform a photogrammetric survey of the case study church represented a cost-efficient on-site data gathering campaign, that does not require contact with the surfaces and can be rapidly used even during a seismic sequence. A complete in-site geometrical survey of a complex building such as a church could be performed in a few hours by moving most of the survey into post-processing operations (e.g., creation of the high-density point cloud);
- *Step 2*: The use of HBIM-based modeling effectuated an optimal interoperability between step 1 (i.e., point cloud development) and step 3 (FEM). Furthermore, the parametric modeling integrated data coming from different sources (e.g., the point cloud, the mechanical material properties, the geometry of the macro-blocks, the results of previous provisional risk assessment, and the structural model) and to store them in a single file reducing the risk of loss of information between the different steps; and
- *Step 3 and 4*: The use of FEM analysis effectuated the detailed seismic assessment of a very complex structure. The modal analysis, which can be carried out by most experienced structural engineers, was used to identify the most highly stressed macro-blocks in an earthquake scenario. The forces and moments demand could be easily obtained via modal response spectrum analysis, exported, and used to classify the failure mechanisms of the masonry piers. Eventually, the stress condition of the shell elements in the FEM was used to identify the most-likely yield lines of the local collapse mechanisms establishing a logical connection between FEM analysis and the more appropriate, but highly sensitive on the

mechanism selection, macro-block modeling approach. The simplified linear modal response spectrum analysis was further checked via an enhanced non-linear pushover SAA resulting in a validation of the identified main collapse mechanism. However, the behavior factor, q_h, prescribed by MIT [42] for URM ordinary buildings was larger than the one obtained for the collapse prevention performance point through the comparison of the capacity curve for the SDoF system with the demand spectrum. Other sources [62, 44] suggested that smaller values for the behavior factor that might be more appropriate for the modeling of churches. The authors encourage for further research on the topic for allowing a larger number of practicing engineers to be able to approach the simplified modeling of complex URM buildings such as churches.

Although the proposed four-step framework may be improved in terms of automatization of the process and accuracy of the results, the authors forecast that it might serve as a useful methodology for the detailed analysis of complex, historic URM buildings that can be applied by the practicing engineering community. The authors also encourage further research on the interaction of HBIM-based and FEM-based software as, while the .ifc files permit discrete interoperability between the geometric and the structural modeling software, the current state of the art requires the engineers either to oversimplify the modeling or to perform significant manual adjustments when exporting the model from one software to the other.

Acknowledgments

This research was primarily funded by a Global Gateways Faculty Research Award at the University of Notre Dame (grant FY18RGG03). Undergraduate students at the University of Notre Dame who assisted with the surveys include Elizabeth DePaola, Emily Brady, Lily Polster, Marie Bond, and Patricia Dirlam. These students were supported by research scholarship funding from various programs, institutes, and centers at the University of Notre Dame, including the Fitzgerald Institute for Real Estate, the Grand Challenges Scholars Program, the Women in Engineering Program, and the Flatley Center for Undergraduate Scholarly Engagement.

The authors are thankful for the assistance of the cultural heritage offices of the involved dioceses, as well as the assistance of Dr. Federica Romiti (diocese of Anagni – Alatri), the Bishop Stefano Manetti and the Surveyor Marco Cortellessa (diocese of Montepulciano – Chiusi – Pienza), Don Francesco Valentini and the Dr. Giovanna Bandinu (diocese of Orvieto – Todi), the Arch. Agapito Fornari (diocese of Palestrina), Don Riccardo Pascolini (diocese of Perugia – Città della Pieve), Don Fabio Sottoriva (diocese of Vicenza), the Dr. Monia Sartori (archdiocese of Trento), the Arch. Graziana Santamaria, and the Surveyor Marco Cherubini. The first author would like to thank his parents Valter Pirchio and Lorena Trentini for their assistance with logistics, as well as an undergraduate student at the University of Trento, Chiara Meloni. The following priests are thanked for granting access to their churches and for assisting during the data collection:

- Diocese of Anagni – Alatri: Deacon Massimiliano Floridi, Don Alessandro De Sanctis, Don Antonio Castagnacci, Don Pierino Giacomi, Don Roberto Martufi, Don Virginio De Rocchis, and the parishes' collaborators.
- Diocese of Montepulciano – Chiusi – Pienza: Don Andrea Malacarne, Don Antonio Nutarelli, Don Azelio Mariani, Don Carlo Sensani, Don Elia Sartori, Don Francesco Monachini, Don Kishor Uppalapati, Don Manlio Sodi, Don Sergio Graziani, Don Silvano Nardi, Don Stefano Cinelli, and the parishes' collaborators.
- Diocese of Nocera Inferiore – Sarno: Friar Damiano Antonino, Friar Felice Petrone, Friar Michele Alfano, Friar Raffaele Panopio, Friar Renato Sapere, and the parishes' collaborators.
- Diocese of Orvieto – Todi: Don Claudio Calzoli, Don Jeremiah Joseph Kelly, Don Marcello Sargeni, Don Marco Gasparri, Don Piero Grassi, and Don Zeffiro Tordi.
- Diocese of Palestrina: Monsignor Andrea Lonardo (diocese of Rome), Don Davide Maria Martinelli, and the parishes' collaborators.

- Diocese of Perugia – Città della Pieve: Don Augusto Martelli, Don Fabio Quaresima, Don Gianni Pollini, Don Giuseppe Piccioni, Don Marco Merlini, Don Matteo Rubechini, Don Vincenzo Esposito, and the parishes' collaborators.
- Diocese of Sorrento – Castellammare di Stabia: Don Antonino Lazzazzara, Don Beniamino Di Martino, Don Ciro Esposito, Don Maurizio Esposito, and the parishes' collaborators.
- Diocese of Trento: Don Ferdinando Murari, Don Maurizio Toldo, and the parishes' collaborators.
- Diocese of Vicenza: Don Adriano Preto Martini, Don Fabio Ogliani, Don Francesco Strazzari, Don Giacomo Viali, Don Giovanni Campagnolo, Don Giovanni Imbonati, Don Giovanni Sandonà, Don Giuseppe Mattiello, Don Luigi Spadetto, Don Paolo Zampiva, and the parishes' collaborators.

References

[1] A. Cagnana, "La transizione al Medioevo attraverso la storia delle tecniche murarie: dall'analisi di un territorio ad un problema sovraregionale," in *I Congresso Nazionale di Archeologia Medievale*, Pisa, 1997.

[2] A. Marotta, Goded, T., S. Giovinazzi, S. Lagomarsino, D. Liberatore, L. Sorrentino and J. M. Ingham, "An inventory of unreinforced masonry churches in New Zealand," *Bulletin of New Zealand Society for Earthquake Engineering*, vol. 48, no. 3, pp. 170-189, 2015.

[3] F. Doglioni, A. Moretti and V. Petrini, Le chiese e il terremoto. Dalla vulnerabilità constatata nel terremoto del Friuli al miglioramento antisismico nel restauro. Verso una politica di prevenzione., Trieste: Edizioni Lint, 1994.

[4] G. Proietti, "Dopo la polvere". Rilevazione degli interventi di recupero (1985-1989) del patrimoni artistico-monumentale danneggiato dal terremoto del 1980-1981, Roma: Istituto Poligrafico e Zecca dello Stato, 1994.

[5] F. Doglioni, Codice di pratica (Linee Guida) per la progettazione degli interventi di riparazione, miglioramento sismico e restauro dei beni architettonici danneggiati dal terremoto umbro-marchigiano del 1997, vol. 15, Tipolitografia DBS, 2000.

[6] S. Lagomarsino and S. Podestà, "Seismic vulnerability of ancient churches: II. Statistical analysis of surveyed data and methods for risk analysis.," *Earthquake Spectra,* vol. 20, no. 2, pp. 395-412, 2004.

[7] G. P. Cimellaro, I. P. Christovasilis, A. M. Reinhorn, A. De Stefano and T. Kirova, "L'Aquila Earthquake of April 6, 2009 in Italy: Rebuilding a Resilient City to Withstand Multiple Hazards," MCEER, 2010.

[8] F. da Porto, B. Silva, C. Costa and C. Modena, "Macro-scale analysis of damage to churches after earthquake in Abruzzo (Italy) on April 6, 2009," *Journal of Earthquake Engineering,* vol. 16, no. 6, pp. 739-758, 2012.

[9] S. Lagomarsino, "Damage assessment of churches after l'Aquila earthquake (2009)," *Bulletin of Earthquake Engineering,* vol. 10, no. 1, pp. 73-92, 2012.

[10] M. Valente and G. Milani, "Seismic response and damage patterns of masonry churches: Seven case studies in Ferrara, Italy," *Engineering Structures,* vol. 177, pp. 809-835, 2018.

[11] M. Valente and G. Milani, "Damage survey, simplified assessment, and advanced seismic analyses of two masonry churches after the 2012 Emilia earthquake.," *International Journal of Architectural Heritage,* vol. 13, no. 6, pp. 901-924, 2018.

[12] L. Hofer, P. Zampieri, M. A. Zanini, F. Faleschini and C. Pellegrino, "Seismic damage survey and empirical fragility curves for churches after the August 24, 2016 Central Italy earthquake.," *Soil Dynamics and Earthquake Engineering,* vol. 111, pp. 98-109, 2018.

[13] A. Penna, C. Calderini, L. Sorrentino, C. F. Carocci, E. Cescatti, R. Sisti, A. Borri, C. Modena and A. Prota, "Damage to churches in the 2016 central Italy earthquakes," *Bulletin of Earthquake Engineering,* vol. 17, no. 10, pp. 1-28, 2019.

[14] D. Pirchio, K. Q. Walsh, E. Kerr, I. Giongo, M. Giretton, B. D. Weldon, L. Ciocci and L. Sorrentino, "Seismic Risk Assessment and Intervention Prioritization for Italian Medieval Churches (in review)," *International Journal of Architectural Heritage,* 2020a.

[15] B. Quelhas, L. Cantini, J. M. Guedes, F. da Porto and C. Almeida, "Characterization and reinforcement of stone masonry walls," *In Structural Rehabilitation of Old Buildings,* pp. 131-155, 2014.

[16] A. Pir, L. S. Hogan, D. Y. Dizhur, K. Q. Walsh and J. M. Ingham, "A comparison of numerically and experimentally obtained in-plane responses of a full-scale unreinforced masonry building frame," in *Tenth Pacific Conference on Earthquake*, Auckland, 2015.

[17] S. Lopez, M. D'Amato, M. Laterza and P. B. Lourenço, "Simplified Formulations for Estimating the Main Frequencies of Ancient Masonry Churches.," *Frontiers in Built Environment,* vol. 5, pp. 18.1-18.15, 2019.

[18] D. Pirchio, K. Q. Walsh, E. Kerr, I. Giongo, M. Giaretton, B. D. Weldon, L. Ciocci and L. Sorrentino, "Aggregated Non-destructive Test Technique for the Assessment of Mechanical Properties of Unreinforced Masonry Italian Medieval Churches (in review)," *Construction and Building Materials*, 2020b.

[19] D. P. Abrams, O. AlShawa, P. B. Lourenço and L. Sorrentino, "Out-of-plane seismic response of unreinforced masonry walls: conceptual discussion, research needs, and modeling issues," *International Journal of Architectural Heritage*, vol. 11, no. 1, pp. 22-30, 2017.

[20] K. Q. Walsh, D. Y. Dizhur, I. Giongo, H. Derakhshan and J. M. Ingham, "Effect of boundary conditions and other factors on URM wall out-of-plane behaviour: design demands, predicted capacity, and in situ proof test results," *Sesoc Journal*, vol. 30, no. 1, p. 57, 2017.

[21] C. Achille, A. Adami, S. Chiarini, S. Cremonesi, F. Fassi, L. Fregonese and L. Taffurelli, "UAV-Based Photogrammetry and Integrated Technologies for Architectural Applications - Methodological Strategies for the After-Quake Survey of Vertical Structures in Mantua (Italy)," *Sensor*, vol. 15, no. 7, pp. 15520-15539, June 2015.

[22] S. Daftry, C. Hoppe and H. Bischof, "Building with Drones: Accurate 3D Facade Reconstruction using MAVs," in *IEEE International Conference on Robotics and Automation*, Seattle, 2015.

[23] M. Faltynovà, E. Matouskovà, J. Sedina and K. Pavelka, "Building Facade Documentation Using Laser Scanning and Photogrammetry and Data Implementation into BIM," *The International Archives of the Photogrammetry, Remote Sensing and Spatial Information Sciences*, vol. 41, no. B3, pp. 215-220, June 2016.

[24] C. Andreotti, D. Liberatore and L. Sorrentino, "Identifying Seismic Local Collapse Mechanisms in Unreinforced Masonry Buildings through 3D Laser Scanning.," *Key Engineering Materials,* vol. 628, p. 79–84., 2015.

[25] L. Sorrentino, M. Doria, V. Tassi and M. A. Liotta, "Performance of a Far-Field Historical Church during the 2016-2017 Central Italy Earthquakes.," *Journal of Performance of Constructed Facilities,* 2019.

[26] T. Luhmann, S. Robson, S. Kyle and J. Boehm, Close-range photogrammetry and 3D imaging, Walter de Gruyter, 2013.

[27] C. Dore and M. Murphy, "Integration of Historic Building Information Modeling (HBIM) and 3D GIS for recording and managing cultural heritage sites.," in *18th International Conference on Virtual Systems and Multimedia,* 2012.

[28] A. Osello, Il futuro del disegno con il BIM per ingegneri e architetti, The future of Drawing with BIM for Engineers and Architects., Palermo: Dario Flaccovio Editore, 2012.

[29] D. Oreni, R. Brumana, A. Georgopoulos and B. Cuca, "HBIM for conservation and management of built heritage: Towards a library of vaults and wooden bean floors.," *ISPRS annals of photogrammetry, remote sensing and spatial information sciences,* vol. 5, pp. 215-221, 2013.

[30] X. Y. Deng and T. P. Chang, "Creating structural model from IFC-based architectural model.," in *Joint International Conference on Computing and Decision Making in Civil and Building Engineering,* Montreal, 2006.

[31] A. Marotta, S. Sorrentino, D. Liberatore and J. M. Ingham, "Vulnerability Assessment of Unreinforced Masonry Churches Following the 2010-2011 Canterbury Earthquake Sequence," *Journal of Earthquake Engineering,* vol. 21, no. 6, pp. 912-934, 2017.

[32] F. Gàlvez, S. R. Abeling, K. Ip, S. Giovinazzi, D. Dizhur and J. M. Ingham, "Using the Macro-element Method to Seismically Assess Complex URM Buildings," in *10th Australian Masonry Conference*, Sydney, 2018.

[33] D.P.C.M. 9 febbraio, *Valutazione e riduzione del rischio sismico del patrimonio culturale con riferimento alle Norme tecniche per le costruzioni di cui al D.M. 14/01/2008*, 2011.

[34] K. Ip, D. Dizhur, L. Sorrentino, M. Masia, M. Griffith and J. Ingham, "Critical review of numerical modelling techniques for seismic response of complex URM buildings.," in *10th Australasian Masonry Conference*, Sydney, 2018.

[35] P. A. Cundall, "A computer model for simulating progressive, large scale movements in blocky rock systems.," in *Proceedings of the international symposium on rock fractures*, 1971.

[36] J. V. Lemos, "Assessment of the ultimate load of a masonry arch using discrete elements.," *Computer methods in structural masonry,* vol. 3, pp. 294-302, 1995.

[37] P. B. Lourenço, "Computational strategies for masonry structures.," Delft University of Technology, 1996.

[38] O. AlShawa, L. Sorrentino and D. Liberatore, "Simulation Of Shake Table Tests on Out-of-Plane Masonry Buildings. Part (II): Combined Finite-Discrete Elements.," *International Journal of Architectural Heritage,* vol. 11, no. 1, pp. 79-93, 2017.

[39] G. Angjeliu, D. Coronelli and G. Cardani, "Structural modelling of complex historic masonry buildings.," in *10th International Masonry Conference*, Milan, 2018.

[40] M. Valente and G. Milani, "Advanced numerical insights into failure analysis and strengthening of monumental masonry churches under seismic actions," *Engineering Failure Analysis,* vol. 103, pp. 410-430, 2019.

[41] F. Galvez, S. Segatta, M. Giaretton, K. Walsh, I. Giongo and D. Dizhur, "FE and DE modelling of out-of-plane two way bending behaviour of unreinforced masonry walls.," in *16th European Conference on Earthquake Engineering*, Thessaloniki, Greece, 2018.

[42] MIT, *Aggiornamento delle "Norme tecniche per le costruzioni"*, Roma: Gazzetta Ufficiale della Repubblica Italiana, 2018.

[43] MIT, *Istruzioni per l'applicazione dell'«Aggiornamento delle "Norme tecniche per le costruzioni"» di cui al decreto ministeriale 17 gennaio 2018*, Roma: Gazzetta Ufficiale della Repubblica Italiana, 2019.

[44] American Society of Civil Engineers, *ASCE 41-17,* Reston, VA: ASCE, 2017.

[45] L. Binda, A. Saisi and C. Tedeschi, "Compatibility of materials used for repair of masonry buildings: research and applications.," in *Binda, L., Saisi, A., & Tedeschi, C. (2006). Masonry. In Fracture and failure of natural building stones (pp. 167-182). Springer, Dordrecht.*, Dordrecht, Springer, 2006, pp. 167-182.

[46] L. Sorrentino, D. Bruccoleri and M. Antonini, "Structural Interpretation of Post-Earthquake (19th Century) Retrofitting on the Santa Maria Degli Angeli Basilica, Assisi, Italy.," in *Sixth International Conference on Structural Analysis of Historic Construction*, Bath, 2008.

[47] J. F. Labuz and A. Zang, "Mohr–Coulomb failure criterion.," *Rock mechanics and rock engineering,* vol. 45, no. 6, pp. 975-979, 2012.

[48] G. Milani and P. B. Lourenço, "A discontinuous quasi-upper bound limit analysis approach with sequential linear programming mesh adaptation.," *International Journal of Mechanical Sciences,* vol. 51, no. 1, pp. 89-104, 2009.

[49] G. Milani, "Upper bound sequential linear programming mesh adaptation scheme for collapse analysis of masonry vaults.," *Advances in Engineering Software,* vol. 79, pp. 91-110, 2015.

[50] A. Chiozzi, N. Grillanda, G. Milani and A. Tralli, "UB-ALMANAC: an adaptive limit analysis NURBS-based program for the automatic assessment of partial failure mechanisms in masonry churches.," *Engineering Failure Analysis,* vol. 85, pp. 201-220, 2018.

[51] G. Milani, E. Milani and A. Tralli, "Upper Bound limit analysis model for FRP-reinforced masonry curved structures. Part I: Unreinforced masonry failure surfaces.," *Computers & structures,* vol. 87, no. 23-24, pp. 1516-1533, 2009.

[52] G. Magenes and G. M. Calvi, "In-plane seismic response of brick masonry walls.," *Earthquake engineering & structural dynamics,* vol. 26, no. 12, pp. 1091-1112, 1997.

[53] M. Tomaževič, Earthquake-resistant design of masonry buildings., London: Imperial College Press, 1999.

[54] Euorpean Committee for Standardization, *EN 1996-1-1:2012,* Brussels: Euorpean Committee for Standardization, 2012.

[55] M. Vinci, Metodi di calcolo e tecniche di consolidamento per edifici in muratura., Palermo: Dario Flaccovio Editore, 2012.

[56] M. Valente and G. Milani, "Damage assessment and collapse investigation of three historical masonry palaces under seismic actions.," *Engineering Failure Analysis,* vol. 98, pp. 10-37, 2019.

[57] M. Valente and G. Milani, "Damage assessment and partial failure mechanisms activation of historical masonry churches under seismic actions: three case studies in Mantua.," *Engineering Failure Analysis,* vol. 92, pp. 495-519., 2018.

[58] G. Milani, M. Valente and C. Alessandri, "The narthex of the Church of the Nativity in Bethlehem: a non-linear finite element approach to predict the structural damage.," *Computers & Structures,* vol. 207, pp. 3-18, 2018.

[59] A. De Boer, "Design strategy structural concrete in 3D focusing on uniform force results and sequential analysis.," Delft University of Technology, Delft, Neatherlands, 2010.

[60] K. Shakeri, M. A. Shayanfar and M. Mohebbi Asbmarz, "A spectra-based multi modal adaptive pushover procedure for seismic assessment of buildings," in *The 14th World Conference on Earthquake Engineering*, Beijing, China, 2008.

[61] G. Milani and M. Valente, "Comparative pushover and limit analyses on seven masonry churches damaged by the 2012 Emilia-Romagna (Italy) seismic events: Possibilities of non-linear finite elements compared with pre-assigned failure mechanisms.," *Engineering Failure Analysis,* vol. 47, pp. 129-161, 2015.

[62] New Zealand Society for Earthquake Engineering and Structural Engineering Society New Zealand, *NZSEE*, NZSEE, 2016.

Index of the Figures

Index of the Tables